Dr. MONISHA CHAKRABORTY / International Journal of Engineering Research and Applications (IJERA) ISSN: 2248-9622 www.ijera.com
Vol. 2, Issue 6, November- December 2012, pp.1292-1301

Comparative Study on Retinal Blood Vessel Detection

Dr. MONISHA CHAKRABORTY
Assistant Professor, School of Bio-Science & Engineering, Jadavpur University, 188, Raja S. C. Mallik Road, Kolkata-700032, India

ABSTRACT

In this work, an algorithm has been developed for automatic detection of blood vessels in normal and abnormal retinal images. The algorithm comprises of four steps: second derivative Gaussian function filtering, local entropy thresholding, median filtering and length filtering. The algorithm so developed has been tested on twenty ocular fundus images. The results of this algorithm are compared with those obtained from other methods. Other methods which are considered in this work for comparison are algorithm as described in [15], imageJ and Hand labeled ground truth segmentation. The comparative results reveal that the algorithm developed in this work is efficient with respect to its accuracy, speed, simplicity and PSNR values. Statistical two-way analysis of variance (ANOVA) is also performed on the comparative results.

Keywords: length filtering; local entropy thresholding; median filtering; ocular fundus images; PSNR values; retinal blood vessels; second derivative Gaussian; two-way analysis of variance (ANOVA).

I INTRODUCTION

Detection of blood vessels in retinal images helps physicians to diagnose ocular diseases and it is used for patient screening, clinical evaluation and grading disease severity [1-3]. Eye is a unique region of the human body where the vascular condition can be directly observed in-vivo. Along with the fovea and optic disc, the vascular tree constitutes one of the main features of an ocular fundus image and several of its properties are distinctly affected by diseases such as diabetes, hypertension, and arteriosclerosis [1, 3]. Other eye diseases, such as choroidal neovascularization, central retinal arterial occlusion and proliferative diabetic retinopathy, etc., also induce changes in the retinal vasculature [4]. In general retinal images are influenced by all factors that affect body vasculature.

When the vascular network is complex, or the number of images is large, manual measurement can become error prone, tiresome or even impossible, and moreover it suffers from operator subjectivity. So, the viable solution to this problem is to use computerized analysis. A group of researchers [5] used an edge detection-based method to extract blood vessel boundaries. In edge detection algorithms, based on enhancement/thresholding method, the discontinuities in the image gray tone are enhanced by neighborhood operators [6]. Robert's operator is the simplest type of differential operator and it consists of 2 x 2 convolution kernels [6]. Prewitt and Sobel operators [7] are improvements on Robert's operator. All these operators yield good results when the edges are sharp. But, the most widely used smoothing filters are Gaussian filters and these filters play the important role in edge and line detection in human visual system [8]. In vessel tracking method, each vessel segment is defined by three attributes: direction, width, and center point [9]. The density distribution of cross section of a blood vessel is modeled using Gaussian function. Individual segments are identified using a search procedure which tracks the center of the vessel and makes decisions about the most probable path of the vessel based on certain vessel properties. This method requires the beginning and ending search points for each vessel which are manually selected. A threshold probing technique is proposed in [2] where the matched-filter-response (MFR) image is used for mapping the vascular tree. A set of criteria is tested to determine the threshold of the probed region and from this it is decided whether the area being probed is a blood vessel or not. Since the MFR image is probed in a spatially adaptive way, different thresholds can be applied throughout the image for mapping blood vessels. Several other works are reported in [10-13] on retinal image processing.

In this paper, an algorithm has been developed to accurately locate and extract blood vessels in ocular fundus images. The results are qualitatively and quantitatively compared with other methods. Other methods which are considered in this work for comparison are: algorithm as described in [15], edge detection module of ImageJ [14] and hand labeled ground truth segmentation. The comparative results reveal that the developed algorithm is efficient with respect to its accuracy, speed, simplicity and PSNR values.

II MATERIALS AND METHODS

The algorithm developed in this work for detection of blood vessels in retinal images comprises of four steps: second derivative Gaussian function

filtering, local entropy thresholding, median filtering and length filtering. Two-dimensional second derivative Gaussian function kernel is convolved with the original image to enhance the blood vessel. Local entropy thresholding is applied to keep the spatial structure of vascular tree segments. Median filtering is used to remove the outliers without reducing the sharpness of image. Length filtering is used to remove misclassified pixels. Ocular Fundus images are RGB images and these are first converted to gray monochrome images. Fig.1 shows the steps of the algorithm developed in this work. Performance evaluation of the algorithm developed in this work has been made by comparing the results obtained from this algorithm with the results obtained from the edge detection module of ImageJ [14], with the results obtained from the algorithm described in [15] and with the results of hand-labeled ground truth segmentation.

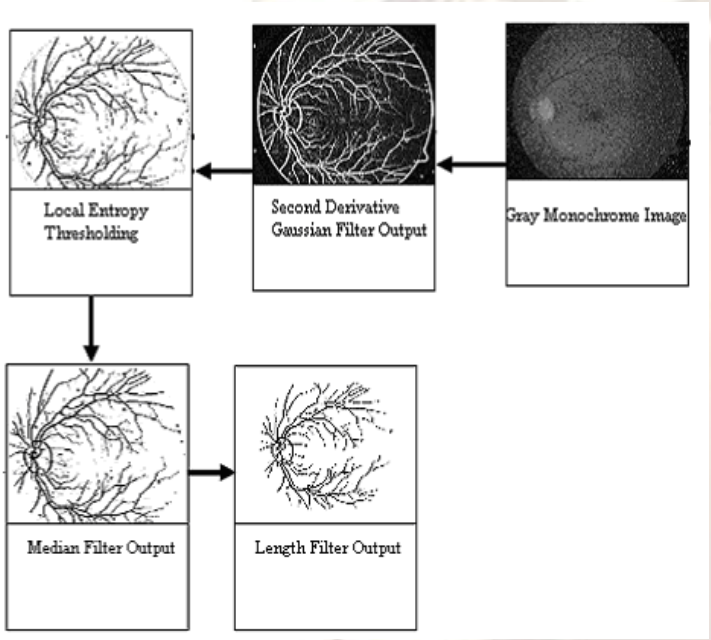

Fig 1: Steps of the algorithm developed in this work

2.1 Derivatives of Gaussian Function

Gaussian derivative model provides edge and line enhancement. A special line weight function (LWF) for enhancing edges in digital images is discussed in [8]. This operator is a combination of Gaussian function and its second derivative, or equivalently, zero and second-order Hermite functions [8].

The Hermite function of order 'n', h_n, with scale parameter 'σ', is given in Eq. (1)

$$h_n(\frac{x}{\sigma}) = \frac{1}{\sqrt{2^n n!}} \frac{d^n}{d(\frac{x}{\sigma})^n} \frac{1}{\sigma\sqrt{\pi}} \exp[-\frac{x^2}{2\sigma^2}] \quad (1)$$

where

$h_0(\frac{x}{\sigma})$ is defined by

$$h_0(\frac{x}{\sigma}) = \frac{1}{\sigma\sqrt{\pi}} \exp[-\frac{x^2}{2\sigma^2}] \quad (2)$$

The different values on 'n' correspond to different order derivatives of Gaussian-like function. Based on empirical optimization of the final vascular tree, 'n' = 2 appears to be optimal.

The model is extended to two dimensions by assuming that a vessel has a fixed width and direction for a short length. The gray-level profile of the cross section of a blood vessel can be approximated by a Gaussian shaped curve [6]. The two dimensional second derivative Gaussian function kernel is designed to convolve with the original image in order to enhance the blood vessel.

A prototype second derivative Gaussian function kernel is expressed in Eq. (3).

$$f(x,y) = -\frac{1}{\sigma^3\sqrt{8\pi}}(x^2-\sigma^2)\exp[-\frac{x^2}{2\sigma^2}], \quad \text{for } |y| \le \frac{L}{2} \quad (3)$$

Where, L is the length of the segment for which the vessel is assumed to have a fixed orientation. Here the direction of the vessel is assumed to be aligned along the y-axis [6, 15]. A blood vessel may be oriented at any angle θ ($0 \le \theta \le \pi$). So, when the Gaussian second derivative function is applied to two dimensional images, it needs to be rotated for all possible angles. The corresponding responses are compared, and for each pixel only the maximum response is retained. A normal retinal image is shown in Fig. 2(a) which has low contrast difference between blood vessels and background. Its second derivative Gaussian function result is shown in Fig. 2(b), here it is seen that the blood vessels are significantly enhanced.

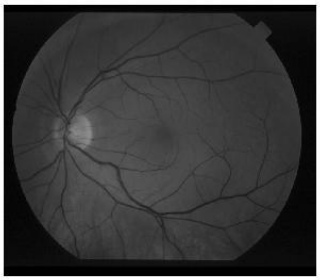

Fig. 2(a) Gray monochrome normal retinal image

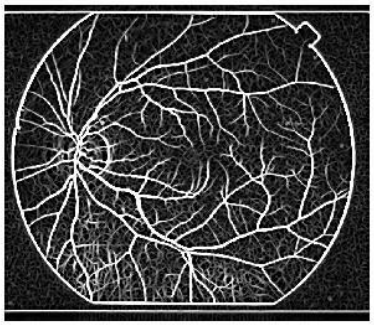

Fig. 2(b) Result of second derivative Gaussian kernel

2.2 Local Entropy Thresholding

Second derivative Gaussian function result is processed further by a proper thresholding scheme in order to extract the blood vessel segments from the background. For this purpose a local entropy thresholding algorithm [15-18] that takes into account the spatial distribution of gray levels has been implemented. The co-occurrence matrix of the image is a P x Q dimensional matrix $T = [t_{ij}]_{P \times Q}$ that gives an idea about the transition of intensities between adjacent pixels, indicating the spatial structural information of an image. Depending upon the ways in which the gray level i follows gray level j, different definitions of co-occurrence matrix are possible. Here, the co-occurrence matrix is made asymmetric by considering the horizontally right and vertically lower transitions. Thus, t_{ij} is defined as given in Eq. (4).

$$t_{ij} = \sum_{t=1}^{P} \sum_{k=1}^{Q} \delta \tag{4}$$

where,

$$\delta = 1 \quad if \quad \left\{ \begin{array}{c} f(l,k) = i \ and \ f(l,k+1) = j \\ or \\ f(l,k) = i \ and \ f(l+1,k) = j \end{array} \right\}$$

$$\delta = 0 \quad otherwise \tag{5}$$

The probability of co-occurrence p_{ij} of gray levels i and j can therefore be written as given in Eq. (6).

$$p_{ij} = \frac{t_{ij}}{\sum_{i} \sum_{j} t_{ij}} \tag{6}$$

If $s, 0 \le s \le L-1$ is a threshold, then s can partition the co-occurrence matrix into four quadrants, namely A, B, C, and D as shown in Fig. 2(c).

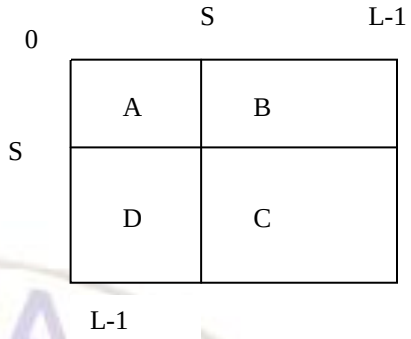

Fig.2 (c) Quadrants of Co-occurrence Matrix

The following quantities are defined as given in Eq. 7(a) and Eq. 7(b).

$$P_A = \sum_{i=0}^{s} \sum_{j=0}^{s} p_{ij} \tag{7a}$$

$$P_C = \sum_{i=s+1}^{L-1} \sum_{j=s+1}^{L-1} p_{ij} \tag{7b}$$

Normalizing the probabilities within each individual quadrant, such that the sum of the probabilities of each quadrant equals to one and the following cell probabilities for different quadrants are obtained as given in Eq. (8),

$$P_{ij}^{A} = \frac{p_{ij}}{P_A} = \frac{t_{ij} / (\sum_{i=0}^{L-1} t_{ij})}{\sum_{i=0}^{s} \sum_{j=0}^{s} t_{ij} / \sum_{i=0}^{L-1} \sum_{j=0}^{L-1} t_{ij}}$$

$$= \frac{t_{ij}}{\sum_{i=0}^{s} \sum_{j=0}^{s} t_{ij}} \tag{8}$$

$$for \ 0 \le i \le s, 0 \le j \le s$$

Similarly,

$$P_{ij}^{C} = \frac{p_{ij}}{P_C} = \frac{t_{ij}}{\sum_{i=s+1}^{L-1} \sum_{j=s+1}^{L-1} t_{ij}} \tag{9}$$

$$for \quad s+1 \le i \le L-1, s+1 \le j \le L-1$$

The second-order entropy of the object can be defined as given in Eq. (10)

$$H_A^{(2)}(s) = -\frac{1}{2} \sum_{i=0}^{s} \sum_{j=0}^{s} P_{ij}^{A} \log_2 P_{ij}^{A} \tag{10}$$

Similarly, the second-order entropy of the background can be written as given in Eq. (11)

$$H_C^{(2)}(s) = -\frac{1}{2} \sum_{i=s+1}^{s} \sum_{j=s+1}^{s} P_{ij}^{C} \log_2 P_{ij}^{C} \tag{11}$$

Hence, the total second-order local entropy of the object and the background can be written as given in Eq. (12)

$$H_T^{(2)}(s) = H_A^{(2)}(s) + H_C^{(2)}(s) \qquad (12)$$

The gray level corresponding to the maximum of $H_T^{(2)}(s)$ gives the optimal threshold for object-background classification. For the second derivative Gaussian function result shown in Fig. 2(b), the local entropy thresholding result is shown in Fig. 2(d) where it can be seen that the blood vessels are clearly segmented from the background.

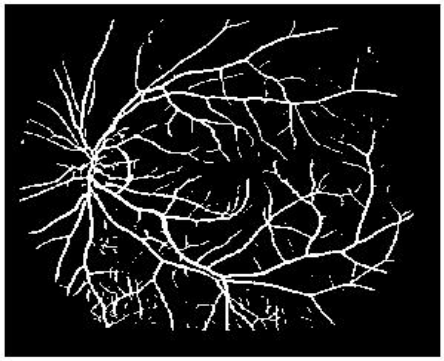

Fig. 2(d) Local entropy thresholding result

2.3 Median Filtering

Two-dimensional median filtering is a nonlinear operation and it has been used to reduce noise and to preserve the edges. For the local entropy thresholding result shown in Fig. 2(d), the two-dimensional median filtering result is shown in Fig. 2(e). The noise in this result has reduced as compared to the earlier step.

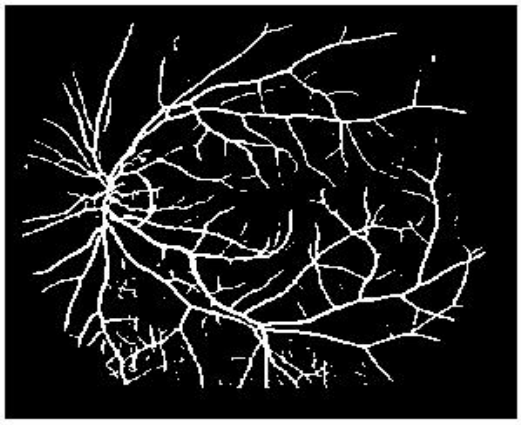

Fig. 2(e) Median filtering result

2.4 Length Filtering

There are still some misclassified pixels in the image, as seen in Fig. 2(e). A clean and complete vascular tree structure is obtained by implementing length filtering technique as reported in [15]. Length filtering is used to remove isolated pixels by using the concept of connected pixels labeling. Connected regions correspond to individual objects. In the length filtering algorithm, implemented in this work, only the resulting classes that exceed a certain number of pixels, e.g., 160, are labeled as blood vessels. Fig. 2(f) shows the result after length filtering where the clear image of the vascular tree structure is obtained.

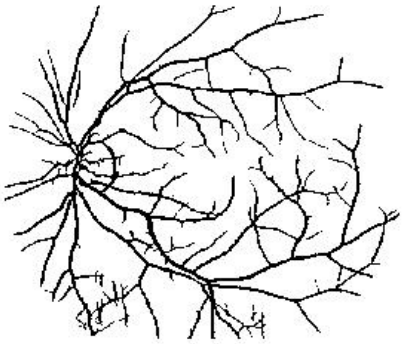

Fig. 2(f) Length filtering result

III RESULTS

On Windows XP, Pentium 4, CPU 1.7 GHz. using MATLAB version 7, the computational time of the whole process of this developed algorithm takes approximately 1 minute for each retinal image. A set of twenty normal and abnormal retinal JPEG images of 605 x 700 pixels, 32 (RGB) with file size of 150 KB are collected from Disha Eye Hospital, Barrackpore, India. The images are taken by Zeiss Fundus FF 450 ^{plus} camera. In order to evaluate the performance of the algorithm developed in this work, comparisons of the results of this algorithm have been made with other methods and the sample results are shown in this section. Comparisons between retinal blood vessel detection methods as considered in this work are done with respect to PSNR values. PSNR values for normal and abnormal retinal images are given in Table 1 as sample results. Two-way ANOVA is performed on the values as shown in Table-1 and the corresponding results are tabulated in Table-2. Summary of comparative results are tabulated in Table 3.

In this work, retinal images are classified into two broad categories; normal and abnormal retinal

images. Fig 3(a) shows the gray monochrome normal retinal image. Fig 3(b) shows the result of the algorithm developed in this work, showing the vascular tree structure of the normal retinal image. Fig 3(c) shows the result obtained from the algorithm described in [15]. Fig 3(d) shows the result obtained from edge detection module of ImageJ. The hand labeled ground truth segmentation is manually done in this work. Fig 3(e) shows the hand labeled ground truth segmentation result for the normal retinal image.

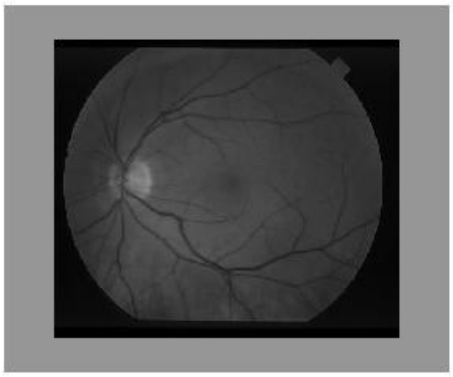

Fig. 3(a) Gray monochrome normal retinal image

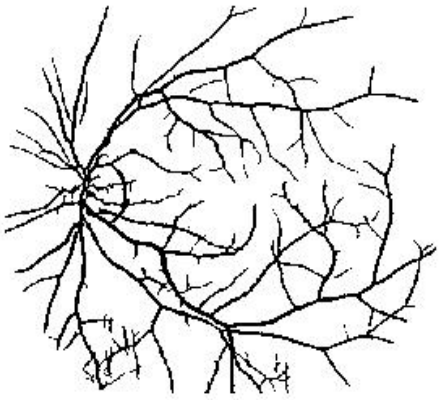

Fig. 3(b) Result obtained from the algorithm developed in this work

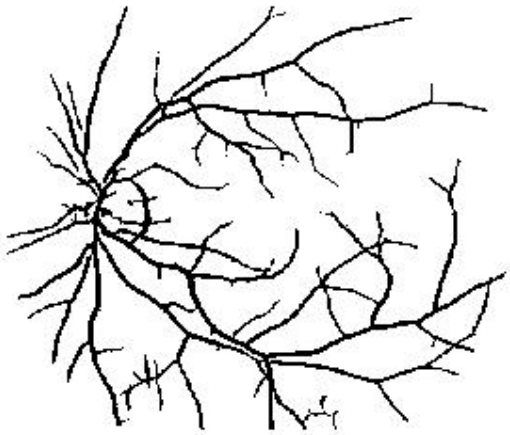

Fig. 3(c) Result obtained from the algorithm in [15]

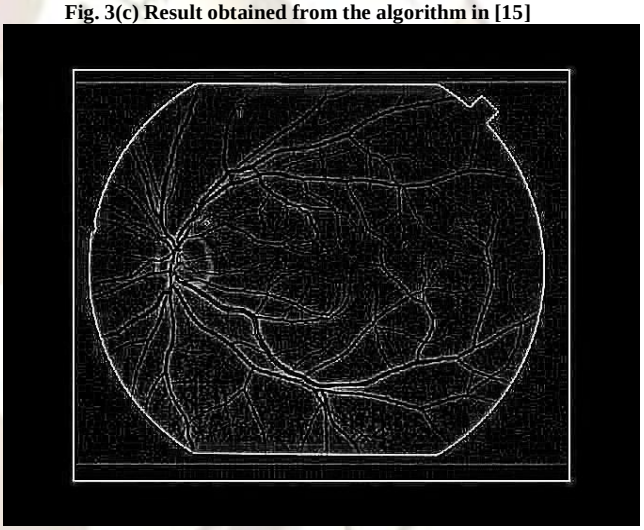

Fig. 3(d) Result obtained from edge detection module of ImageJ

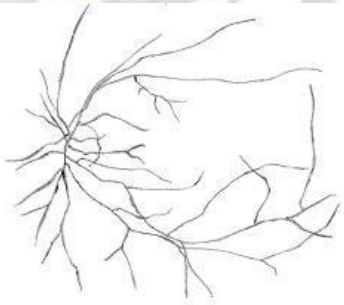

Fig. 3(e) Hand labeled ground truth segmentation result

Fig. 4 shows the results for abnormal retinal images. Under abnormal retinal images three cases e.g. choroidal neovascularization, central retinal arterial occlusion and proliferative diabetic retinopathy have been considered. The first column of Fig. 4 shows results for the abnormal retinal image e.g. choroidal neovascularization. The second column of Fig. 4 shows results for the abnormal retinal image e.g. central retinal arterial occlusion. The third column of Fig. 4 shows results for the abnormal retinal image e.g. proliferative diabetic retinopathy.

The first row of Fig. 4 shows the gray-monochrome abnormal retinal images. The second row of Fig. 4 shows the hand-labeled ground truth segmentation results which are manually done in this work. The third row of Fig. 4 shows the results obtained from edge detection module of ImageJ. The fourth row of Fig. 4 shows the results of the algorithm developed in this work and the fifth row of Fig. 4 shows the results obtained from the algorithm in [15].

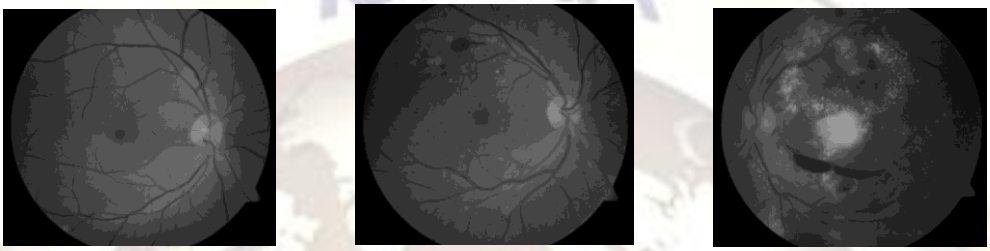

(a) (f) (k)

Fig 4(a), Fig. 4(f), Fig. 4(k) First row: Gray monochrome abnormal retinal images

(b) (g) (l)

Fig 4(b), Fig. 4(g), Fig. 4(l) Second row: Hand labeled ground truth segmentation results

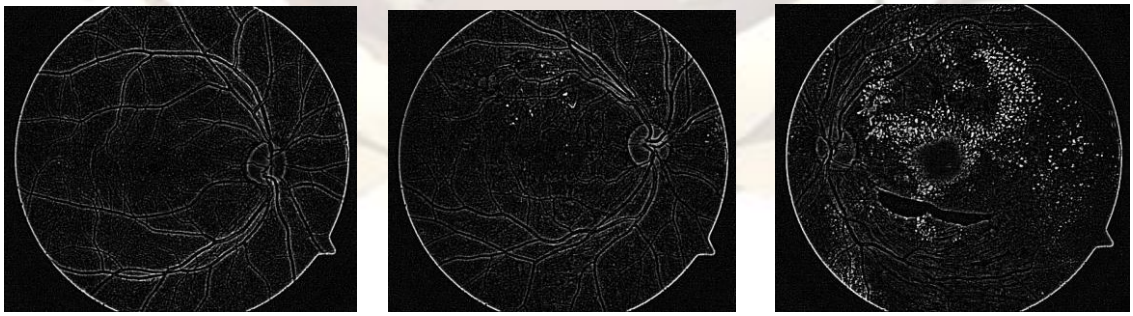

(c) (h) (m)

Fig 4(c), Fig. 4(h), Fig. 4(m) Third row: Results obtained from edge detection module of ImageJ

(d) (i) (n)

Fig 4(d), Fig. 4(i), Fig. 4(n) Fourth row: Results obtained from the algorithm developed in this work

(e) (j) (o)

Fig 4(e), Fig. 4(j), Fig. 4(o) Fifth row: Results obtained from the algorithm in [15]

Table-1: Comparison with respect to PSNR values

Automatic Retinal Blood Vessel Detection Methods Compared with Hand-labeled Ground Truth Segmentation Result	PSNR values (dB)			
	Type of Retinal Image			
	Normal	Choroidal Neovascularization	Central Retinal Arterial Occlusion	Proliferative Diabetic Retinopathy
Algorithm developed in this work	60.5517	59.5745	59.2754	57.1826
Algorithm as per [15]	60.8884	59 .6555	58.6309	57.4315
Edge detection module of ImageJ	62.6307	48.2178	48.2044	48.2831

PSNR values are obtained by comparing the results obtained from each method with hand labeled ground truth segmentation result for each image considered in this work. From Table-1, it is observed that the PSNR values obtained using the algorithm developed in this work are in good agreement with those obtained using the other methods. Two-Way ANOVA is performed on the values as shown in Table-1 and the result so obtained is shown in Table-2.

Table-2: Two Way ANOVA

Source	SS	df	MS	F	p-value
Columns	90.0028	3	30.0009	2.309	0.1762
Rows	142.684	2	71.342	5.491	0.0441
Error	77.9573	6	12.9929		
Total	310.6441	11			

The observed value of 'F' for "Automatic Retinal Blood Vessel Detection Methods" is 5.491 and this value is larger than the corresponding tabulated value for df (2, 6). So, this is significant at 5% level i.e. there is significant difference between the three methods. The p-value is 0.0441. Also, from the calculations of critical difference between the totals for the three Automatic Retinal Blood Vessel Detection Methods it has been found that the Edge detection module of ImageJ differs from the algorithm developed in this work and Edge detection module of ImageJ differs from the algorithm as described in [15]. Algorithm developed in this work and the algorithm as described in [15] gives similar result. The algorithm developed in this work incorporates second derivative Gaussian function filtering whereas the method reported in [15] has considered Matched filter response of the input image. Moreover, the algorithm developed in this work incorporates median filtering which reduces noise. But this filtering technique is not present in the method described in [15]. So, the algorithm developed in this work can be considered as an alternative method for detecting retinal blood vessels from normal and abnormal retinal images.

The observed value of 'F' for "Type of retinal image" is 2.309 and this value is less than the corresponding tabulated value for df (3, 6). So, this is not significant at 5% level i.e. there are no significant differences between the types of retinal images with respect to PSNR values and p-value is 0.1732.

Table 3: Summary of Performances

S.No.	Retinal Blood Vessel Detection Method	Fine Structure Detection Accuracy	Smaller Blood Vessel Detection Accuracy	Outer Edge/Boundary	Operator Subjectivity	Speed of Execution
1	Hand labeled ground truth segmentation	Medium	Medium	Absent	Present	Slow
2	Edge detection module of ImageJ	Fairly good	Fairly good	Present	Absent	Very fast
3	Algorithm as per [15]	Very good	Very good	Absent	Absent	Fast
4	Algorithm developed in this work	Very good	Very good	Absent	Absent	Fast

IV Discussions

Results of this paper reveal that second derivative Gaussian function enhances the contrast of blood vessels against the background. Local entropy thresholding algorithm takes into account the spatial distribution of gray levels. It performs efficiently in distinguishing between enhanced blood vessel segments and the background. It preserves the structural details of retinal images. Median filtering suppresses outliers without compromising the sharpness of the image and length filtering minimizes misclassified pixels.

Fig. 3(b) shows the result of the algorithm developed in this work for the normal retinal image as shown in Fig. 3(a). Fig. 3(c) shows the result of the algorithm as described in [15]. From Fig. 3(b) and Fig. 3(c) it can be observed that smaller blood vessels are prominent in both these figures. Fig. 3(d) shows the result from edge detection module of ImageJ. From Fig. 3(b) and Fig. 3(d), it can very well be seen that the fine structures are more clearly visible and these fine structures are more prominent in Fig. 3(b) than the same in Fig. 3(d). Moreover, it can be observed that Fig. 3(d) contains an outer edge/boundary along with the detected blood vessels. This is the weakest point for the results obtained from edge detection module of ImageJ. The result of the algorithm developed in this work is better than that of ImageJ because here one can detect clearly the blood vessels which have the diagnostic importance and not the outer edge/boundary. Fig. 3(e) shows the hand labeled ground truth segmentation result. From Fig. 3(b) and Fig. 3(e) it can be very well seen that fine structure details of retinal blood vessels are very much prominent in Fig. 3(b) than the result seen in Fig. 3(e). Moreover, the method of hand-labeled ground truth

segmentation suffers from the problem of operator subjectivity.

Fig. 4(d), Fig. 4(i) and Fig. 4(n) show the results obtained from the algorithm developed in this work for the abnormal retinal images shown in Fig. 4(a), Fig. 4(f) and Fig. 4(k) respectively. Fig. 4(e), Fig. 4(j) and Fig. 4(o) show the results obtained from the algorithm described in [15] for the same set of abnormal retinal images which are shown in Fig. 4(a), Fig. 4(f) and Fig. 4(k) respectively as mentioned above. From Fig. 4(d) and Fig. 4(e); Fig. 4(i) and Fig. 4(j); Fig. 4(n) and Fig. 4(o) it can very well be seen that the fine structures and the smaller blood vessels are prominent in these results. So, these results imply that the algorithm developed in this work is giving comparable results.

Fig. 4(c), Fig. 4(h) and Fig. 4(m) show the results obtained from edge detection module of ImageJ for the abnormal retinal images shown in Fig. 4(a), Fig. 4(f) and Fig. 4(k) respectively. From Fig. 4(c) and Fig. 4(d); Fig. 4(h) and Fig. 4(i); Fig. 4(m) and Fig. 4(n) one can very well see that the fine structures are more clearly visible and these fine structures are more prominent in the results of the algorithm developed in this work. Moreover, it can be observed that Fig. 4(c), Fig. 4(h) and Fig. 4(m) contain outer edge/boundary along with the detected blood vessels. These are the short comings in the results obtained from the edge detection module of ImageJ. But, the algorithm developed in this work can detect only the blood vessels which have the diagnostic importance and not the outer edge/boundary. The algorithm developed in this work performs better than edge detection module of ImageJ.

Fig. 4(b), Fig. 4(g) and Fig. 4(l) show the hand labeled ground truth segmentation results for the abnormal retinal images shown in Fig. 4(a), Fig. 4(f) and Fig. 4(k) respectively. From Fig. 4(b) and Fig. 4(d); Fig. 4(g) and Fig. 4(i); Fig. 4(l) and Fig. 4(n) one can very well see that fine structure details of the retinal blood vessels are much more prominent in Fig. 4(d), Fig. 4(i) and Fig. 4(n). Moreover, the method of hand-labeled ground truth segmentation suffers from the problem of operator subjectivity and this is a time consuming method.

From Table-1 it is seen that the PSNR values obtained from the algorithm developed in this work and those obtained from the algorithm as described in [15] are in good agreement to each other. Results of Two-way ANOVA are tabulated in Table-2. The comparative performances of the algorithms for retinal blood vessel detection as discussed in this paper are summarized in Table 3.

V CONCLUSION

This study infers that the algorithm developed in this work is very much useful and efficient for automatic, accurate and fast detection of blood vessels from both normal and abnormal retinal images. The results obtained from this developed algorithm are in good agreement with those obtained from other methods.

ACKNOWLEDGEMENTS

Author wishes to acknowledge the help and cooperation of Disha Eye Hospital, Barrackpore, India for providing ocular fundus images.

REFERENCES

[1]. T. W. Hansen, J. Jeppesen, S. Rasmussen, H. Ibsen and C. T. Pedersen, Ambulatory blood pressure and mortality: A population-based study, *Hypertension, 45*, 2005, 499–504.

[2]. A. Hoover, V. Kouznetsova and M. Goldbaum Locating blood vessels in retinal images by piecewise threshold probing of a matched filter response, *IEEE Trans. Medical imaging, 19*, 2000, 203-210.

[3]. T. Teng, M. Lefley and D. Claremont, Progress towards automated diabetic ocular screening: a review of image analysis and intelligent systems for diabetic retinopathy, *Medical & Biological Engineering & Computing, 40*, 2002, 1-13.

[4]. Ocular fundus images collected from Eye Hospital, Barrackpore, Kolkata-700120, West Bengal, India.

[5]. A. Pinz, S. Bernogger, P. Datlinger and A. Kruger, Mapping the human retina, *IEEE Trans. Medical imaging,17*, 1998.

[6]. S. Chaudhuri, S. Chatterjee, N. Katz, M. Nelson and M. Goldbaum, Detection of blood vessels in retinal images using two-dimensional matched filters, *IEEE Trans. Medical imaging, 8*, 1998.

[7]. W. K. Pratt, *Digital Image Processing*, New York: Wiley: 1978.

[8]. L. M. Kennedy and M. Basu, Image Enhancement using a human visual system model, *Pattern Recognition, 30*, 1997, 2001-2014.

[9]. L. Zhou, M. S. Rzeszotarski, L. Singeman and I. M. Chokreff, The detection and quantification of retinopathy using digital angiograms, *IEEE Trans. Medical imaging, 13*, 1994.

[10]. M. J. Johnson and G. Dougherty, Robust measures of three-dimensional vascular tortuosity based on the minimum curvature of approximating polynomial spline fits to the

vessel mid-line, *Medical Engineering and Physics,29*, 2007, 677-690.

[11]. Z. M. Rodriguez, P. Kenny and L. Gaynor, Improved characterization of aortic tortuosity, *Medical Engineering and Physics, 33*, 2011, 712-719.

[12]. M. Garcia, M. I. Lopez, D. Alvarez and R. Hornero, Assessment of four neural network based classifiers to automatically detect red lesions in retinal images, *Medical Engineering and Physics, 32*, 2010, 1085-1093.

[13]. C. I. Sanchez, R. Hornero, M. I. Lopez M. Aboy, J. Poza and D. Abasolo, A novel automatic image processing algorithm for detection of hard exudates based on retinal image analysis, *Medical Engineering and Physics,30*, 2008, 350-357.

[14]. Weblink: http://rsbweb.nih.gov/ij/index.html

[15]. T. Chanwimaluang and G. Fan, An efficient blood vessel detection algorithm for retinal images using local entropy thresholding, *IEEE Transactions*, 2003.

[16]. N. R. Pal and S. K. Pal, Entropic thresholding, *Signal processing,16*, 1989, 97-108.

[17]. S. K. Pal, N. R. Pal, Object Extraction from image using Higher order Entropy, *IEEE Transactions*, 1988.

[18]. N. R. Pal and S. K. Pal, Entropy: A New Definition and its Applications, *IEEE transactions on systems, man, and cybernetics*, *21*, 1991.